Numerical Characterization of Natural Swirling Flame Evolving in Free Environment via FDS: a Comprehensive Investigation of Fires Problems

M. Al. Thamri[1], T. Naffouti[1,2], S. Gannouni[1] and J. Zinoubi [1,2†]

[1]University of Tunis El-Manar, Faculty of Sciences of Tunis, Department of Physics, Laboratory of Energizing and Thermal and Mass Transfer, 2092, El-Manar, Tunis, Tunisia
[2]University of Tunis El-Manar, Preparatory Institute for Engineering Studies El-Manar, 2092, El-Manar, Tunis, Tunisia

†*Corresponding Author Email: jamil.zinoubi@ipeiem.utm.tn (Jamil ZINOUBI)*

ABSTRACT

In this paper, a numerical study of a swirling flame generated through the interaction between a central fire and its surrounding fires is performed. A swirling flame can be configured by installing a secondary's sources surrounding the central source, organized in an asymmetrical manner in order to ensure circumferential entrainment of the central flame by the supply puffs air. An analysis is performed to study this kind of flow. This analysis highlights the different zones that characterize the vertical propagation of a swirling flame; a first zone, close to the fire source, characterized by an acceleration of the flow and an increase of the temperature. A second zone marked by the passage of the temperature by a maximum while changing variation with a net decrease of the flow acceleration and a third zone where the thermal and dynamic fields change and gradually decrease. Moreover, this study shows an axisymmetric flow behavior with two different aspects of its global structure. A central region characterized by a block motion (solid core) where the flow is rotational, characterized by a concentration of vorticity, and surrounded by the rest of the space where the flow is irrotational. Moving vertically away from the active source, results show an attenuation of the axial vortex intensity which is accompanied by a disappearance of movement by block. The centerline evolution of the axial and azimuthal momentum flux enables also to highlight these different aspects of the global flow structure.

Keywords: Swirling flame; Solid core; Vorticity; Rankine vortex Model; Momentum flux; Swirl number.

NOMENCLATURE

C_p	specific heat	V_x	x-direction component of velocity
C_s	smagorinsky constant	V_y	y-direction component of velocity
D^*	characteristic diameter of fire source	V_{xy}	horizontal velocity
g	gravitational acceleration	V_z	axial velocity
G_z	axial momentum flux	V_θ	orthoradial velocity
G_θ	azimuthal momentum flux	w_z	vorticity vertical component
k_t	turbulent thermal conductivity	x, y, z	coordinates directions
P_{rt}	turbulent Prandtl number		
Q	source heat flux		
r_0	heart radius of the rotating flow	**Greek letters**	
S	Swirl number	Δ	filter width in LES
S_{ij}	symmetric rate of stress tensor	Ω	angular velocity
t	time	μ_t	turbulent viscosity
T	flow temperature	ρ	density
T_0	ambient Temperature	$\delta_{x,y,z}$	grid size in directions x, y and z
u	velocity vector		

1. INTRODUCTION

The study of rotating flows is motivated by the large number and variety of applications, natural or industrial, in which they occur. As example, these flows can be found in the hydraulic equipment, turbines, downstream of many rotating devices like wind turbines, rotors helicopters, helical flow burners, in internal aerodynamics particularly in jet engines and combustion systems and also intervene chemistry in mixing devices or separation of components through centrifugation. Also, they can be observed in swirling storms (Tornado) in the geophysical field in fires (fire tornado).

In fires problems, a large amount of experimental and numerical investigations have been performed. Several researchers are focused their attention to generated irrotationnel fire flow observed in forest or buildings and its interaction with surrounding environments (Gustenyov *et al.* 2018 ; Gao *et al.* 2018 ; Jangi and Dlugogorski, 2017 ; Liu *et al.* 2017). Other studies have been carried out on swirling flows/flames/fires. Thus, the effect of rotation on the behavior of these flows must be understood in order to develop possible techniques for extinction of these turning fires. It depends on the flux ratio of the angular momentum which generates the rotation by the flux of axial momentum generated by the buoyancy forces. According to previous studies, several researchers have concentrated to study the behavior of a rotating flame by forced and natural ventilation (Pinto *et al.* (2017); Yuen *et al.* (2018); Parente *et al.* (2019); Lei *et al.* (2019))

Thus, we can cite the work of Lei *et al.*2013, 2015b, who established experimentally a correlation linking the heating power, the flame height and temperature. Moreover, in a rotating fire cases they indicated that the rotating flame is characterized by a significant instability by noting that the entire flame is inclined and rotates about the symmetry axis with the increase of the angular velocity. Yu *et al.* 2013, studied experimentally the effect of the width of the slits through which penetrates the ambient air on the general characteristics of the rotating flow. Xia and Yadigaroglu, 1998, carried out numerical and experimental investigation of strongly swirling flow in a combustion chamber. In the same period, Ide and Ghil, 1997, examined a Rankine vortices related to vortex systems.

By focusing on the scaling laws of the flow structures around geometrically similar fire whirls, Rikya and Kuwana (2019) proposes a methodology to apply laboratory-scale data to predicting the flow structures around real, large-scale fire whirls.

Hartl and Smits (2016) investigate the whirl velocity distributions, and scaling laws for the average whirl height and centerline velocity. Parente *et al.* (2019) were conducted numerical simulations in order to ascertain the effect of circulation on the fire whirl structure.

Zhou *et al.* 2013, analyzed the heat flux effect of an active source on the rotating flame behavior. They noted that the increase in the imposed heat flux promotes the flow supply. The most intense supply air stream drives the flame thereby activating its rotation. They also found a significant improvement in the flame height with the increase of heating flux.

Recently, by conducting an experimental investigation on the effect of imposed circulation on temperature and velocity in general fire whirl, Lei *et al.* (2019) were found that the centerline excess temperature and axial velocity varied consistently with the flame shape. Moreover, Lei *et al.* (2015a, 2015b) were stated that these two parameters increased with height in the continuous flame region while they decreased steadily downstream.

Previous work make a significant scientific contribution in the experimental and numerical study of the rotating flame, yet it reveals the lack crucial information about the creation of a rotating flame by interaction between multiple sources arranged in a particular way.

This type of flow has been studied by Zhou and Wu, 2007. They used a system formed by five sources: a central source surrounded by four secondary sources disposed asymmetrically. They carried out experimental study and numerical simulations using FDS in order to examine the effect of secondary sources positions (slits width) on the behavior of central flow. They noted that the flow of rotation is considerably affected by the slit width variation by showing the existence of an optimum configuration where a high angular acceleration is observed. This study, although it illustrates the generation of a rotating flow following the interaction of these sources, but he did not examine several points associated with the fine structure. Given their high sensitivity to the boundary conditions, rotating flows therefore have a wide variety of phenomena some of which are still unexplained.

Focusing on the above-mentioned research gaps, this paper addresses the characterization of swirling flame evolving in free environment. This study was conducted to provide a deeper understanding of swirling flame dynamics and its formation mechanism.

2. NUMERICAL SIMULATION

The present numerical study uses a CFD software (Fire Dynamic Simulator (FDS)) of vast global interest in fire modeling.

FDS (Fire Dynamic Simulator) is developed as an open source of an international collaborative effort led by the National Institute of Standards and Technology (NIST) and VTT Technical Research Centre of Finland. This tool is a computer program dedicated to study and simulate the dynamics and combustion of fires in domestic or industrial confined buildings and to evaluate the efficiency and performance of the protection means against problems related to fire, such as the distribution of temperature and soot concentration. This software solves numerically a form of the Navier-Stokes

equations appropriate for low Mach number applications, adapted to low speed, thermally-driven flow with an emphasis on smoke and heat transport from fires.

These equations are briefly given here (McGrattan *et al.* 2018):

Mass equations

$$\frac{\partial \rho}{\partial t} + \nabla \cdot (\rho \mathbf{u}) = 0 \tag{1}$$

Momentum equations

$$\rho \left(\frac{\partial u}{\partial t} + (\mathbf{u} \cdot \nabla) \mathbf{u} \right) + \nabla p = \rho g + \mathbf{f} + \nabla \tau \tag{2}$$

Energy equations

$$\frac{\partial (\rho h)}{\partial t} + \nabla \cdot \rho h \mathbf{u} - \frac{Dp}{Dt} = \dot{q}''' - \nabla \cdot q_r + \nabla \cdot k\nabla T + \nabla \cdot \sum_l h_l (\rho D)_l \nabla Y_l \tag{3}$$

Species equations

$$\frac{\partial (\rho Y_l)}{\partial t} + \nabla \cdot \rho Y_l \mathbf{u} = \nabla \cdot (\rho D)_l \nabla Y_l + \dot{m}_l''' \tag{4}$$

Equation of state

$$p = \frac{\rho RT}{\bar{W}} \tag{5}$$

The turbulence is modeled by default by the technique of Large Eddy Simulation (LES). It is possible that the user can perform a Direct Numerical Simulations (DNS). LES model with Smagorinsky subgrid type are retained in this study. The approach of the large eddy simulation is to calculate the large scale eddies and model the small scales dissipative processes (viscosity, thermal conductivity, material diffusivity) (McGrattan *et al.* 2018). The modeling is based on the assumption of the subgrid turbulent viscosity, which is modeled by:

$$\mu_t = \rho (C_S \Delta)^2 \left[2\bar{S}_{ij} : \bar{S}_{ij} - \frac{2}{3} (\nabla \bar{u})^2 \right]^{\frac{1}{2}} \tag{6}$$

Where $\bar{S}_{ij}$ is the symmetric rate of strain tensor which is defined by:

$$\bar{S}_{ij} = \frac{1}{2} \left(\frac{\partial \bar{u}_i}{\partial x_j} + \frac{\partial \bar{u}_j}{\partial x_i} \right) \tag{7}$$

And C_s is the Smagorinsky constant and taken equal to 0.2 the default value used in FDS.

The other diffusive parameters, the thermal conductivity and material diffusivity, are related to the turbulent viscosity by:

$$k_t = \frac{\mu_t C_p}{Pr_t} \tag{8}$$

$$(\rho D)_{l,t} = \frac{\mu_t}{Sc_t} \tag{9}$$

Where Pr_t is the turbulent Prandtl number and Sc_t is the turbulent Schmidt number both assumed constant with the default value in FDS is equal to 0.5.

Upon its public release in 2000, a permanent set of verification and validation cases was maintained

(McGrattan *et al.* 2018). Today, it is at version 6.7. Used extensively by the engineering community of fire modeling, this package has undergone extensive validation testing its performance in several applications and configurations. With FDS, NIST provides to users with a powerful program, called Smokeview, to visualize the development of fire and smoke.

The reliability of a large eddy simulation predictions is probably sensitive to the size and the quality of calculation grid, from where a particular attention to the choice of this parameter and therefore to be considered carefully at first. LES gives reasonable results with a grid size chosen carefully. Specifically, the determination of the grid size is important for the field near to an important gradient place as for example near the site of the fire.

In FDS, to justify the stability of numerical scheme and to estimate the convergence calculation, the courant-Friedrichs-Lewy (CFL) criterion is used. This criterion is related to the convective terms of the governing equation. It is very important for the large-scale calculations where convective transport dominates diffusive. The estimated velocities are tested at each time step, δt , to ensure that the CFL condition is satisfied:

$$\delta t \max \left(\frac{|u_{ijk}|}{\delta x}, \frac{|v_{ijk}|}{\delta y}, \frac{|w_{ijk}|}{\delta z} \right) < 1 \tag{10}$$

The initial time step size is specified automatically in FDS by dividing the size of a mesh cell by the characteristic velocity of the flow. The default value of time step is:

$$\frac{5(\delta x \delta y \delta z)^{\frac{1}{3}}}{\sqrt{gH}} \tag{11}$$

During the calculation, the time step change and constrained by the convective and diffusive transport speeds by ensuring that the CFL condition is satisfied at each time step. The time step will eventually change into a quasi-stationary value when the fire environment will reach a quasi-steady state

In this study, the Swirling flame source is depicted schematically in Fig.1. It is constituted essentially by a hot square block surrounded by a four identical rectangular hot blocks having all the same height. The Four blocks are disposed asymmetrically around the central block in order to supply the central source with air fresh by four openings between secondary blocks. Consequently, it creates a swirling flame which propagates vertically from active source. Hence, the fresh air causes a tangential movement of the fire generated by heaters. It thus creates its rotation around the vertical axis. The blocks are placed on the ground in free environment. All vertical surfaces of different blocks are considered adiabatic and the top surface of each block is subjected to constant flux of $5\ MW.m^{-2}$.

The 3-D computational domain adopted for all simulation is $10 \times 10 \times 20\ m^3$, (xyz), as shown in Fig. 2. Open boundary conditions are assumed for

the all ends of computational domain and an ambient temperature equal to $20°C$ is selected for all tests simulations.
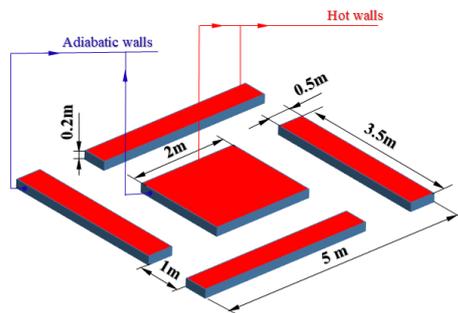

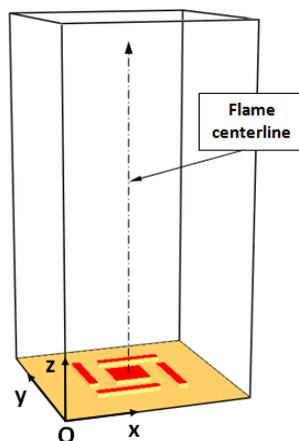**Fig. 1. Schematic view of flame sources positions.**

Fig. 2. Schematic of the numerical setup for a swirling flame simulation.

As mentioned in FDS users' guide, the selection of grid size δx is related to the characteristic diameter of fire source D^* which is defined as follows (McGrattan *et al.* 2017):

$$D^* = \left(\frac{Q}{\rho_0 C_p T_0 \sqrt{g}}\right)^{2/5} \qquad (3)$$

Based on this relationship which indicates that a grid size approximately 10% of the characteristic fire diameter is acceptable to ensure reliable operation of FDS, four different grid sizes as shown in Table 1 are tested in this study. For these tests, the grid size is uniform all directions.

Table 1 Summary of the different tested grid systems

Test no.	Grid number			Total cells	CPU time (hr)
	X	Y	Z		
1	50	50	100	125000	7.38
2	80	80	160	1024000	28.06
3	100	100	200	2000000	102.97
4	120	120	240	3456000	200.02

The vertical distribution of velocity in the median plane of central hot block for the different tested

grid systems presented in Fig. 3 shows that the results become slightly different for tests No. 2-4 and independent of meshes. To economize computation time, the grid size of the test No. 2 is finally used in this work.
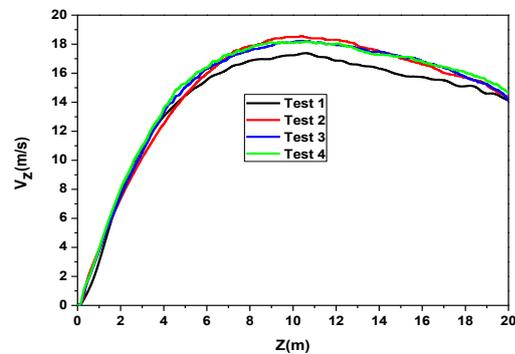

Fig. 3. Axial distribution of vertical component of velocity predicted with the different tested grid systems.

For this grid system, Fig. 4 shows the evolution of CFL number and time step with the iteration number showing thus the satisfaction of calculation convergence of the present FDS simulation. In this study, the FDS simulation is executed up to 120 s. The time evolution of axial velocity at different levels (Z=3, 9 and 15m) shows that the generated flow reaches a quasi-stationary stage at about 40s as shown in Fig.5. Thus, the time interval between 80s and 120s is selects in this study to calculate the average of the studied parameters.
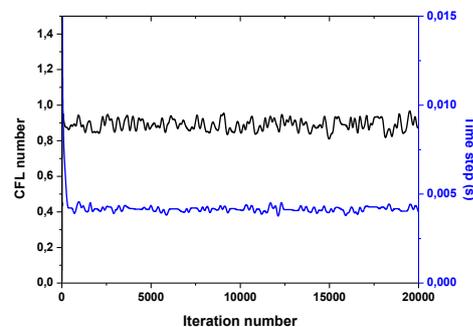

Fig. 4. CFL number and time step evolution for FDS simulations of studied configuration.

In order to check the FDS potentiality in simulation of rotating flows, experience Lei *et al.* 2013, was compared with those obtained by the numerical FDS simulation for different levels (Fig. 6). Examination of this figure shows that numerical profiles follow the overall evolution of experimental profiles. Our results are in good agreement with those of Lei *et al.* 2013, and correctly follow the same variations. The divergence between the numerical and experimental values remains relatively low throughout these levels.
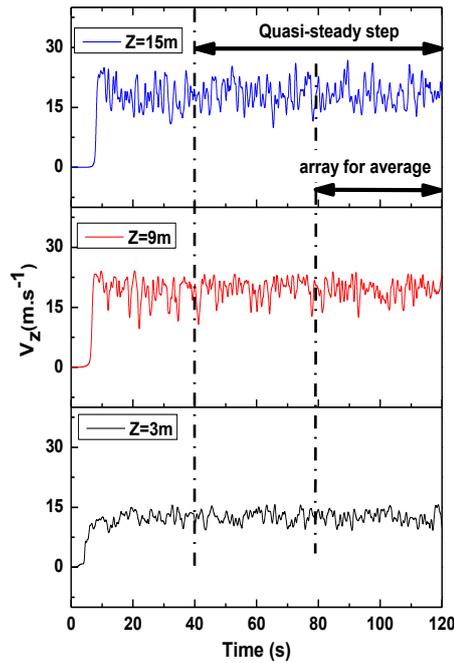
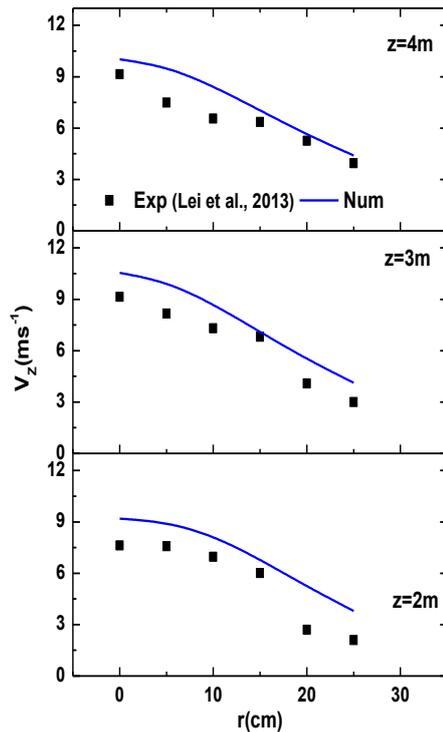**Fig. 5. Time evolution of the vertical component of velocity on the flame centerline for different levels.**

Fig. 6. Comparison of the axial component of flow velocity predicted by FDS to that measured experimentally by J. Lei *et al.*2013.

3. SIMULATION RESULTS AND DISCUSSIONS

3.1. Global View on the Structure of Swirling Flame

As shown in Fig. 7, the isotherms illustrate an overall image of the thermal field giving information on the area occupied by the flame during its ascent. It shows an axisymmetric flow behavior. Close to the generating source there is a tightening of isothermal lines related to high thermal gradients due to a sudden change of the ambient air in hot flame. Away from the heat source, the thermal gradients become weaker. These low gradients are related to the existence of the puffs of supply fresh air coming from the outside environment. This behavior allows us to suppose the existence of two zones of flow in the radial direction; a central recirculation zone (CRZ), surrounded by an external recirculation zone (ERZ). The same behavior is observed by Lei *et al.* (2015b). Moreover, in the vertical direction, Fig. 7 also shows three different behaviors that characterize the propagation of flow. A first zone, close to the source, of fort thermal gradient, called persistent flame zone followed by a second intermediate zone called intermittent flame zone. Just up a third zone called the buoyant plume zone characterized by low gradients where there is a lateral expansion of the flow.
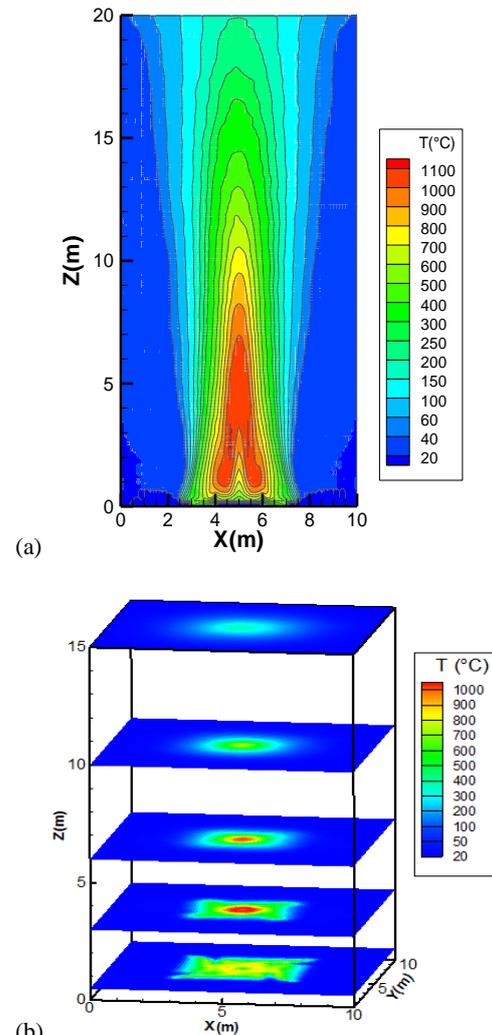

(a)

(b)

Fig. 7. Average thermal field of the generated flow: (a) in the median plane (Y = 5m), (b) in horizontal planes (Z = 0.5, 3, 6, 10 and 15m).

Figure 8 presents flow visualization and tracers particles given by smokeview. This figure gives a good indication on the global flow structure. It provides information on the region occupied by the flame during its ascent and allows to discover the different flow zones. This visualization shows that the flow is regularly supplied with fresh air through all sides. The flow is strongly driven by the tangential supply puffs air coming from the environment, through the openings between the secondary sources. It occurs thus a net rotation of the central flow. Away from the central source, a disappearance of flow rotation is observed for high altitudes. These observations lead us to assume the existence of three distinct zones characterizing the vertical propagation of flow. The first zone shows a development of a strongly rotating flow, influenced by the tangential supply air puffs. This behavior changes completely in the intermediate zone that starts from a height of around 10m, where there is a reduction of the rotation of the flow. Higher, a lateral expansion of the flow is observed.
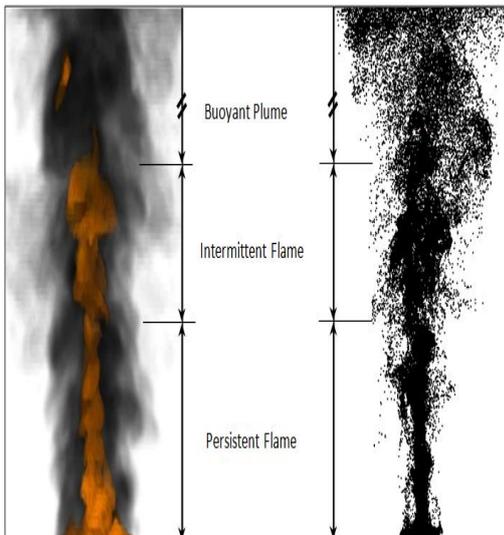

Fig. 8. Flow visualization by smokeview.

Figure 9 shows the iso-velocity and streamline plotted into a flow symmetry plane (xOz). This figure confirms that the generated flow is axisymmetric and highlights the various zones: a low velocity in the area close to the source followed by a strong dynamic gradient while moving away vertically and progressively from it due to an acceleration of flow during its propagation. And then a lateral expansion of flow in the region relatively far away from the generating source.

Furthermore, the streamline confirm that the flow is supplied by fresh air from the environment from all sides.

Figures 10 and 11 show respectively, the orthoradial velocity with streamline for different horizontal planes and the instantaneous vorticity. These figures clearly illustrate the findings

mentioned above and show the formation mechanism of the central vortex. Indeed, due to the very particular position of secondary sources, the air puffs penetrate from the openings between these sources, for driving the central flow tangentially by creating its rotation around its axis. In addition, the results shows a strong rotational flow for the lower altitudes and by moving vertically away from the generating source a progressive decrease of the rotation with a lateral expansion of flow.
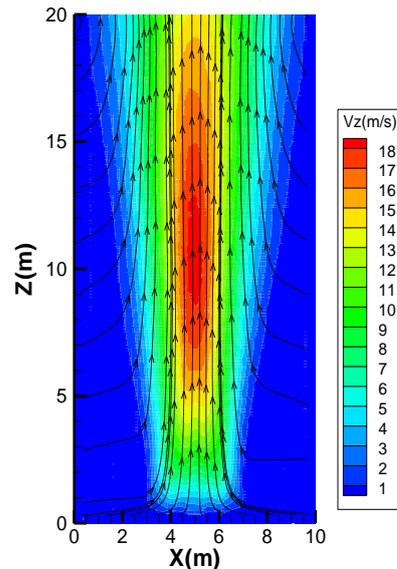

Fig. 9. Average dynamic field in the median plane: iso-velocity with streamlines.

The axial evolution of temperature and vertical component of velocity of the generated flow presented in Fig. 12 shows also the existence of three different behaviors: a first zone close to the source where this later exercises its important effect, for which an acceleration of the flow is observed with an increase in the average temperature until it reaches its maximum. During the vertical propagation of flow, temperature passes through a maximum then it changes variation with a net decrease of the flow acceleration indicating the transition to an intermediate zone. Beyond this region, the thermal and dynamic fields change of variation and decrease progressively indicating a new flow regime where the buoyancy forces are dominant. However the general shape of these profiles is similar to that found by McCaffrey, 1979; Zhou and Wu, 2007. Therefore McCaffrey, 1979, fire plume theory has been extended to describe the swirling flame. The swirling flame is considered to have the same three regimes.

The gross feature of each regime is the same as described by McCaffrey, 1979, for free fire plumes. However the swirling flame shapes are slightly different from a free fire plume. The swirling flame consists of persistent flame zone, the intermittent flame zone and the buoyant plume zone.
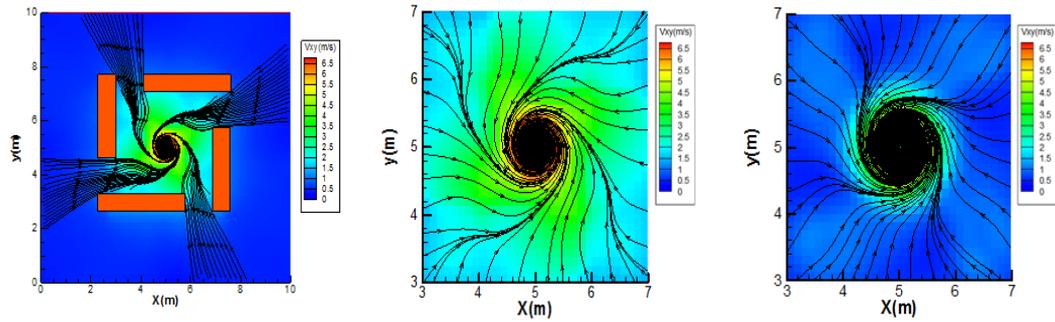
**Fig. 10. Dynamic average field: iso- orthoradial velocity with streamlines in horizontal planes:
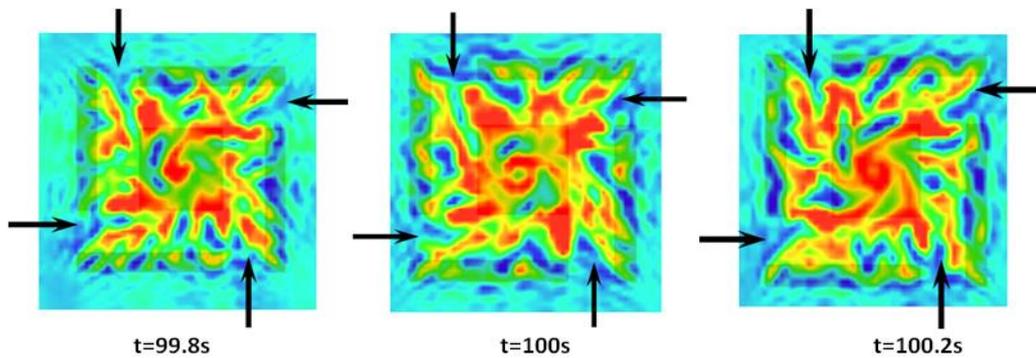(a)   z = 0.5 m, (b) z = 1 m, (c) z = 3 m.**

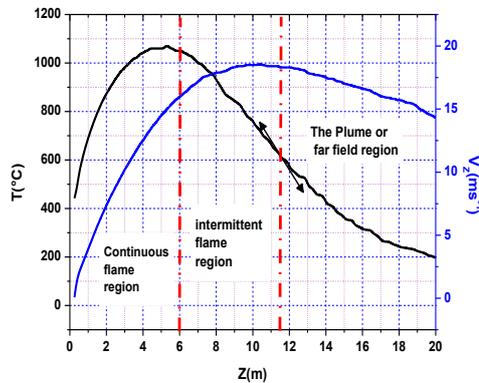**Fig. 11. Instantaneous vorticity: vortex formation.**

Fig.12. Axial evolution of temperature and vertical component of velocity of the generated flow.
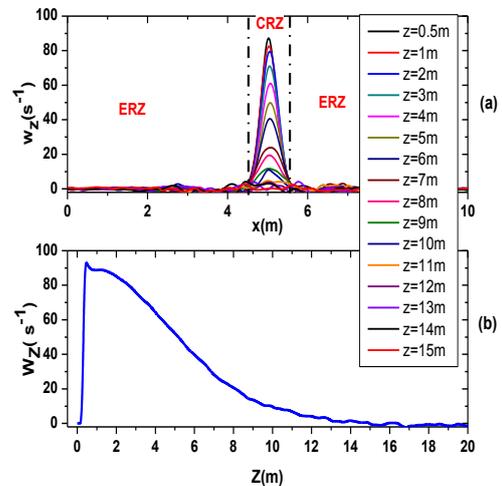

Fig.13. Variation of vertical component of the vortex vector (a) radial evolution, (b) Axial evolution.

Figure 13.a shows the radial evolution of vertical component of the vorticity vector in the median plane for different levels. Two different aspects of the overall flow structure can be noted. A central region (vortex core), wherein the flow is rotational, characterized by a concentration of vorticity

$(W_z > 0)$.This region is surrounded by the rest of space where the flow is almost irrotational. This second zone is characterized by zero values of the vorticity vector. Besides, by moving vertically away from the generating source, the vector vortex decrease indicating finally, at about 15m, the disappearance of rotation, and the transition at an irrotational flow (Fig. 13.b).

3.2. Rankine model checking

Figure 14 shows a comparison between the azimuthal velocity numerically predicted with that obtained by applying the Rankine Vortex model for different levels. This comparison illustrates an increase of the azimuthal velocity from the vortex center, qualitatively similar to the solid rotation part of the Rankine vortex, and a decrease of this velocity after the characteristic distance r_0. The numerical results follow the same overall evolution

of that obtained by the Rankine Vortex model and the discrepancy between the two results remains relatively low for all levels.
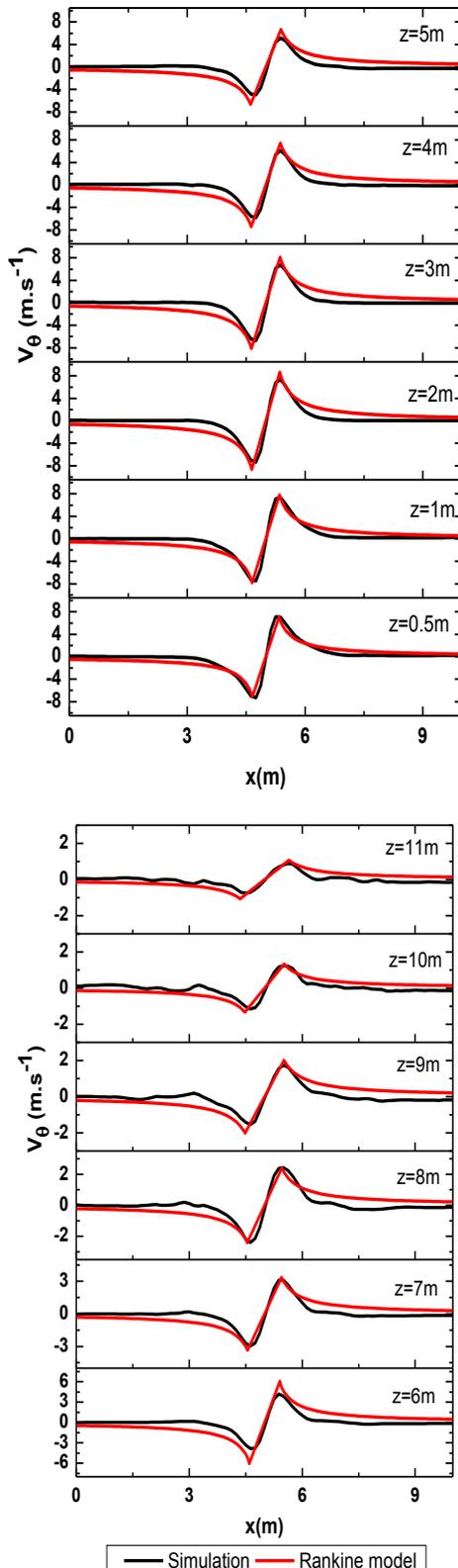

Simulation — **Rankine model**

Fig.14. Comparison between the azimuthal velocity obtained by the simulation with that obtained by applying the Rankine Vortex model.

Figure 15 presents respectively the vertical and radial evolution of the peripheral velocity $V_\theta(r_0)$ and the velocity $V_\theta(r)$ of flow for different z altitudes. This figure confirms the previously mentioned observations for different altitudes. The results shows that the core of flow is a cylinder of radius r_0 and the orthoradial peripheral velocity $V_\theta(r_0)$ progressively decreases as moving away from flame sources. This behavior can be explain by the fact that there is a decrease of flow tangential entrainment by the supply air puffs in the far region.

3.3. Momentum Flux and Swirl Number

Figure 16 shows the axial evolution of the axial momentum flux G_z (i.e. axial thrust) and azimuthal momentum flux G_θ (i.e. angular momentum). These two parameters G_z and G_θ are given by Eldrainy *et al.* (2009):

$$G_z = 2\pi\rho \int_0^{r_0} V_Z^2 r\,dr \qquad (4)$$

$$G_\theta = 2\pi\rho \int_0^{r_0} V_Z V_\theta r^2\,dr \qquad (5)$$

This figure enables to highlight three aspects of the global flow structure. Firstly, significant increases with an almost linear progression of the axial momentum flux in the first zone where the generating source exerts its major effect. This increase is related to a strong acceleration of the upward flow in this region. Thereafter, the axial momentum flux changes of variation until it reaches its maximum, thus indicating the transition by an intermediate zone. Beyond this maximum, it progressively decreases declaring a new regime of flow that occurs. For the angular momentum flux, the predicted result confirms the existence of three region flow during its ascent; this parameter increases during the vertical flame propagation until it reaches its maximum. Thereafter, it decreases progressively until the altitude z = 10 m. Beyond this level, the angular momentum flux change of variation (inflection point) and continues its decrease in becoming zero for high altitudes. This behavior is a direct consequence of the penetration of supply air streams from outside which will entail tangentially the central flame. This air penetration decreases progressively by moving vertically away from the source of the flame. For high altitudes, null values are related to the disappearance of these air puffs.

To characterize a swirling flow, it seems necessary to introduce a parameter that quantifies the importance of rotational movement relative to the convection.

Beer and Chigier (1972) were first to introduce such a parameter: the swirl number S. This number is defined from the angular momentum flux G_θ and the axial momentum G_z by:

$$S = \frac{G_\theta}{r_0 G_z} \qquad (6)$$

As shown in Fig.16, the vertical evolution of the swirl number of flow illustrates high values of this number at the lower altitudes. This is bound to the dominance of axial flux of the tangential

momentum compared with that of the axial momentum. The intensity of angular momentum in this zone is related to the high penetration of air puffs from outside that will entrained tangentially the central flow and thus produce its rotation.
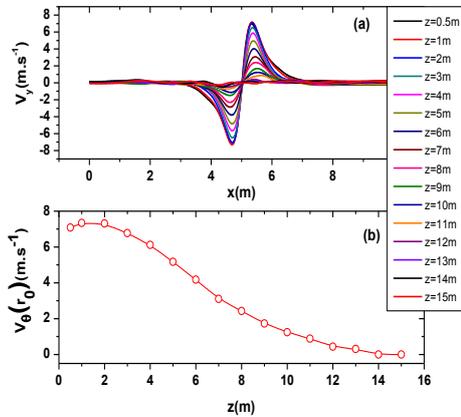

Fig. 15. (a) Radial evolution of the azimuthal velocity for different altitudes z, (b) Vertical evolution of azimuthal peripheral velocity.
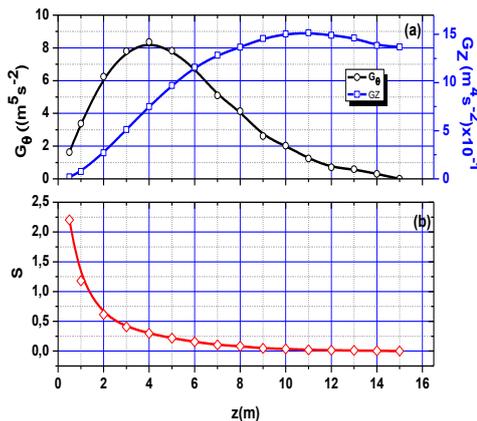

Fig. 16. (a) Axial evolution of the axial momentum flux and the angular momentum flux, (b) Vertical evolution of the swirl number.

During the vertical flow propagation, the swirl number decreases progressively (as 1/z) and becomes zero for high altitudes. In this region, a change in behavior of the angular momentum which decreases progressively is noted whereas the axial momentum continues its increase and becomes predominant in this relatively region away of the source. The flow can be classified in three categories: flow of low swirl (S < 0.6), flow of dual helical (0.6 < S < 1.3) and flow of strong swirl (S > 1.3).

For flow to low swirl number, there appears any recirculation zone. The velocity and temperature profiles of a low swirl flow remain Gaussian to about S < 0.6 (Chigier and Chervinsky, 1967). From S = 0.6 around, it appears a central toroïdal recirculation zone in the flow. An important characteristic of this recirculation zone is that its

center is closer to the source and its size increases as the flow swirl number increases. Figure 17 shows that increasing the swirl number causes a drop of temperature and velocity in the vortex core and that this drop increases.
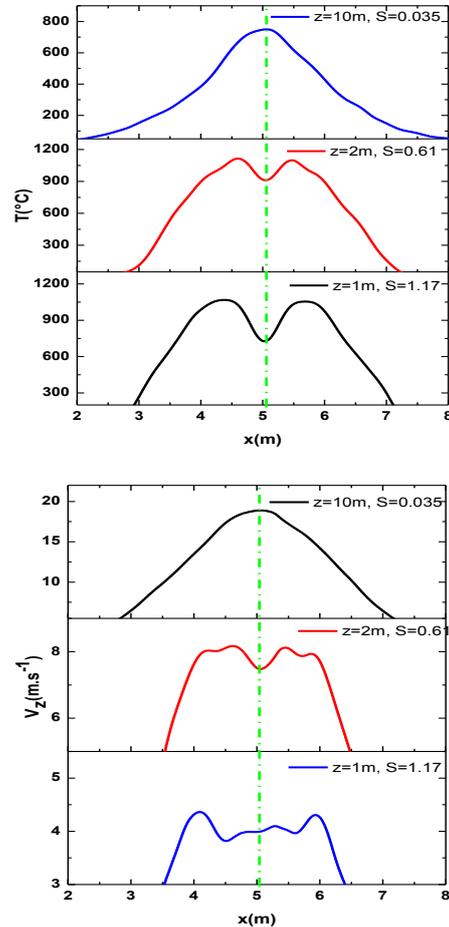

Fig. 17. Temperature and average velocity profiles for different swirl number values.

4. CONCLUDING REMARKS

The present work is a contribution on the characterization of a natural convection flow turning from an active source evolving in a free and unlimited environment through the FDS software.

Examination of thermal and dynamic fields shows an axisymmetric flow behavior. It allows discovering the different areas of flow during its propagation where the flow regime is undergoing significant changes; a first zone close to the source ($Z \leq 6m$), called persistent flame area where the source exerts its major effect, where a strong tangential drive of the central flow is observed with a marked acceleration in the direction of propagation. Also a strong longitudinal thermal gradient is noted in this area. During the vertical propagation of flow, temperature passes through its maximum and then they gradually decrease indicating a new flow regime that is triggered; this intermediate zone called intermittent flame zone ($6m \leq Z \leq 11m$). Moving away from

the source, the velocity reaches its maximum then it change variation. Beyond this region, the dynamic field decreases progressively indicating a new flow regime where the buoyancy forces are dominant ($Z > 11m$). In this region a lateral expansion of the flow is observed which is accompanied by a reduction in thermal gradients until the extinction of the flame. This third area called buoyant plume where buoyant forces are dominant. Besides, the streamlines show that the flow supply fresh air from the surrounding environment, through the openings and along the sides asymmetrically and highlight the driving phenomenon of the central flow by supply air puffs thus causing its rotation around the axis of the primary source.

The vertical evolution of swirl number shows higher values for lower altitudes which related to the dominance of the angular momentum flux relative to that in the axial direction. The intensity of the tangential flux in this area is related to the high current air penetration from outside that will entrained the central flow tangentially and thus produce its rotation. During the flow vertical propagation, the swirl number gradually decreases and becomes zero for the highest levels. In this region there is a change in behavior of the angular momentum flux which decreases gradually as the axial momentum flux continues to increase and becomes dominating in this relatively area far of the source. It can be concluded that the effects of swirl tend to disappear for the high altitudes and have a significant action on the field near the flow source.

Appendix: Rankine vortex

The Rankine vortex is often called a Rankine combined vortex for the reason that it has two separate flow fields Ide and Ghil (1997). It is a circular flow in which the interior flow field (core) involves only an azimuthal velocity which increases linearly with radius from zero along the central axis to a maximum value at a radius (r_0). Thus, this region rotates like a solid body even though it is fluid. The outer flow (tail) is also purely azimuthal with maximum velocity at radius r₀. From this point outward, the velocity declines inversely with radius. Such a flow is called a potential flow because there is a scalar velocity potential function for it the mathematical description of the combined vortex is:

- In this flow kind, a phenomenon similar to that encountered in the tornado will approached. Indeed, a cylinder of radius $'r_0'$ and axis 'z' is considered in which the rotational vector is not zero but outside of the cylinder, a rotational zero will be taken.

- A particularly simple kinematic approach of a tornado will adopted in order to understand its basic mechanisms.

- We therefore place in a Galilean referential that is the terrestrial reference. The cylindrical symmetry of a tornado suggests the model in cylindrical coordinates. The concept of free vortex will be considered (Ide and Ghil, 1997).

- Consider that the fluid inside a cylinder of radius r_0, is rotating around its revolution axis with a peripheral velocity V_θ and the outside fluid is at rest. The fluid in contact with the cylinder (i.e. solid-body rotation) is set in motion by the rotation of the cylinder. The Fluid outside of the cylinder also adopts a rotational movement around the cylinder (entrainment phenomenon).

Therefore describes a tornado as an incompressible flow in cylindrical symmetry about the z axis (vertical axis). The velocity field is orthoradial and the tornado is fixed to the ground and only turn on itself. The vortex vector is modeled as follows:

$$\begin{cases} - Constant\ non\ zero\ for\ r < r_0 \\ \\ -zero\ for\ \ r > r_0 \end{cases} \quad (a.1)$$

It is therefore considered that the vorticity ($\vec{w} = 2\vec{\Omega} = \overrightarrow{rot}\vec{V}$) is homogeneous inside the tornado and it is zero outside.

Applying the Stokes' theorem on a circle of radius r_0:

$$\Gamma = \oint_{(c)} \vec{V}.d\vec{l} = \iint_{(s)} \overrightarrow{rot}\vec{V}.d\vec{S} = \iint_{(s)} \vec{w}.d\vec{S} \quad (a.2)$$

By choosing a circle of radius r as contour (C) oriented in the trigonometrically direction, and (S) a surface building on (C) we obtain:

$$\begin{cases} -for\ \ r < r_0, \ \ \Gamma(r) = 2\pi\ r\ V_\theta(r) = \int_0^r 2\pi r w_z dr \\ \\ -for\ \ r > r_0, \ \ \Gamma_0 = 2\pi\ r\ V_\theta(r) = \ \int_0^{r_0} 2\pi r w_z dr \end{cases} \quad (a.3)$$

So, the orthoradial velocity is given by

$$\begin{cases} -for\ \ r < r_0,\ V_\theta(r) = \frac{\Gamma(r)}{2\pi r} \\ \\ -for\ \ r > r_0, \quad\ \ V_\theta(r) = \frac{\Gamma_0}{2\pi r} \end{cases} \quad (a.4)$$

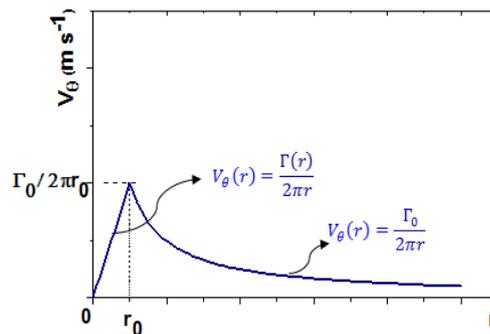Thus, graphically, the orthoradial velocity is shown in Fig.a1.

Fig. a1. Radial evolution of the orthoradial component V_θ of flow velocity: Rankine combined vortex.

Figure a.2 shows the radial evolution of vertical component of vorticity $W_z(r)$ and the azimuthal velocity $V_\theta(r)$. The azimuthal velocity $V_\theta(r)$ is calculated through equations (a.4). The results show that the vorticity is concentrated in the flow core and also allows to distinguish the two zones: an external region (I) which is attached to an interior region (II), seat of vorticity. The vorticity is

concentrated in the region (II) (vortex core) while it is almost zero in the region (I) that corresponds to an irrotationnel flow (potential flow). In region II the effects of viscosity increase gradually as the radius r decreases and the velocity gradient $\frac{\partial v_\theta}{\partial r}$ increases. Below a radius r_0 equal to the core radius, only the block rotational movements are possible. In this case, the angular velocity Ω_0 is constant, the azimuthal velocity is given by $V_\theta(r) = \Omega_0 r$ and this central region is the vortex core.
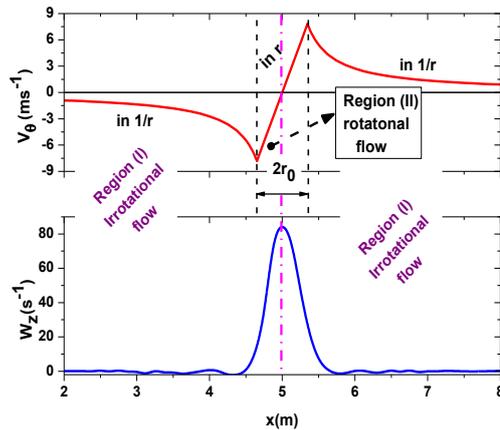

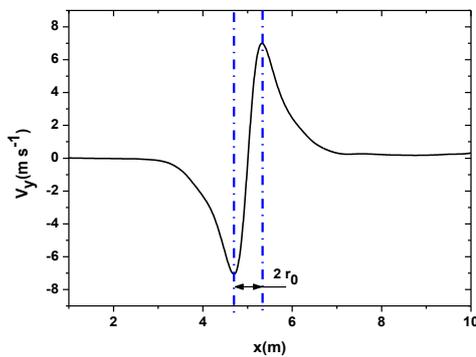**Fig. a 2. Radial evolution of vertical component of the vortex vector and the orthoradial velocity.**

Fig. a 3. Determination of the radius vortex core from the radial evolution of the velocity component V_y.
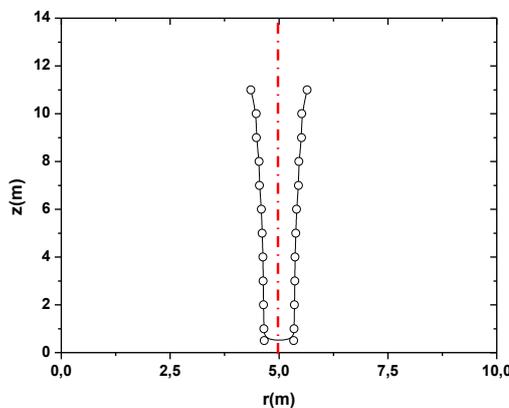

Fig. a 4. Vertical evolution of the extent of the vortex core.

As shown in Fig.a 3 the evolution of the velocity component V_y a function of x shows that this component reaches its extrêma on both side of the flow axis. These extrêma correspond to the peripheral velocity values which is tangent to the vortex core. In these regions the velocity V_y is orthoradial ($V_y(r_0) = V_\theta(r_0)$). The characteristic distance $2r_0$ between the two extrêma depicts the vortex core diameter. By varying the altitude z, the vertical evolution of the extent of vortex core can be determined (Fig.a 4).

REFERENCES

Beér, J. M. and N. A. Chigier (1972). *Combustion Aerodynamics*, Applied Science Publishers (Elsevier) Ltd., London, in the USA, Wiley Publishing Co, p. 265.

Chigier, N. A. and A. Chervinsky (1967). Experimental investigation of swirl vortex motion in jets. *Journal of Fluid Mechanics* 34, 443-451.

Eldrainy, Y. A., H. S. Aly, K. M. Saqr and M. N. M. Jaafar (2009). A Multiple Inlet Swirler for Gas Turbine Combustors. *Proc. of The International Conference on Fluid Mechanics*, Heat Transfer and Thermodynamics, World Academy of Science, Engineering and Technology Tokyo, Japan,.

Gao, W., N. Liu, Y. Jiao, X. Xie, Y. Pan, Z. Li, X. Luo, L. Zhang and T. Ran (2018). Flame length of non-buoyant turbulent slot flame, *Proceedings of the Combustion Institute* 37, 3843-3850.

Gustenyov, N., N. K. Akafuah, A. Salaimeh, M. Finney, S. McAllister and K. Saito (2018). Scaling nonreactive cross flow over a heated plate to simulate forest fires, Combust. *Flame* 197, 340-354.

Hartl, K. A. and A. J. Smits (January 2016). Scaling of a small scale burner fire whirl. *Combustion and Flame* 163, 202-208.

Ide, K. and M. Ghil (1997). Extended Kalman filtering for vortex systems. Part II: Rankine vortices and observing-system design. *Dynamics of Atmospheres and Oceans* 27, 333-350.

Jangi, M. and B. Z. Dlugogorski (2017). On wall fire interaction in a small pool fire: A large-eddy simulation study. *Fire Safety Journal* 92, 199-209.

Lei, J., C. Ji, N. Liu and L. Zhang (2019). Effect of imposed circulation on temperature and velocity in general fire whirl: an experimental investigation. *Proceedings of the Combustion Inst.* 37, 4295-4302.

Lei, J., N. Liu, J. S. Lozano, L. Zhang, Z. Deng and K. Satoh (2013). Experimental research on flame revolution and precession of fire whirls. , *Proceedings of the Combustion Institute* 34,

2607–2615.

Lei, J., N. Liu and K. Satoh (2015a). Buoyant pool fires under imposed circulations before the formation of fire whirls. , *Proceedings of the Combustion Institute* 35, 2503–2510.

Lei, J., N. Liu, L. Zhang and K. Satoh (2015b). Temperature, velocity and air entrainment of fire whirl plume: A comprehensive experimental investigation, *Combustion and Flame* 162, 745–758.

Liu, N., S. Zhang, X. Luo, J. Lei, H. Chen, X. Xie, L. Zhang and R. Tu (2017). Interaction of two parallel rectangular fires. , *Proceedings of the Combustion Institute* 37, 3833-3841.

McCaffrey, B. J. (1979). *Purely Buoyant Diffusion Flames: Some Experimental Results*, NBSIR 79-1910, National Bureau of Standards, Gaithersburg, MD.

McGrattan, K., S. Hostikka, R. McDermott, J. Floyd, C. Weinschenk and K. Overholt (2017). *Fire Dynamics Simulator*: Technical Reference Guide, Volume 1: Mathematical Model. NIST Special Publication 1018-1 (sixth edition).

McGrattan, K., S. Hostikka, R. McDermott, J. Floyd, C. Weinschenk and K. Overholt (2017) *Fire Dynamics Simulator: User's Guide*. NIST Special Publication 1019 (sixth edition).

McGrattan, K., S. Hostikka, R. McDermott, J. Floyd and M. Vanella (2018). *Fire Dynamics Simulator Technical Reference Guide* Volume 3: Validation. NIST Special Publication 1018-3, Sixth Edition.

Parente, R. M., J. M. C. Pereira and J. C. F. Pereira (June 2019). On the influence of circulation on fire whirl height. *Fire Safety Journal* 106, 146-154.

Pinto, C, D. Viegas, M. Almeida and J. Raposo (2017). Fire whirls in forest fires: An experimental analysis. *Fire Safety Journal* 87, 37-48.

Rikiya, Y. and K. Kuwana (2019). Scaling laws of flow structures around geometrically similar fire whirls, *Journal of Thermal Science and Technology* 14(1).

Xia, J. L. and G. Yadigaroglu (1998). Numerical and experimental study of swirling flow in a combustor model, *International Journal of Heat and Mass Transfer* 41, 1485-1497.

Yu, H., S. Guo, M. Peng, Q. Li, J. Ruan, W. Wan and C. Chen (2013). Study on the influence of air-inlet width on fire whirls combustion characteristic. *Procedia Engineering* 62, 813 – 820.

Yuen, A. C., G. H. Yeoh, S. C. Cheung, Q. N. Chan, T. B. Chen, W. Yang and H. Lu (2018). Numerical study of the development and angular speed of a small-scale fire whirl. *Journal of Computational Science* 27, 21-34.

Zhou, K., N. Liu, J. S. Lozano, Y. Shan, B. Yao and K. Satoh (2013). Effect of flow circulation on combustion dynamics of fire whirl. , *Proceedings of the Combustion Institute* 34, 2617–2624.

Zhou, R. and Z. N. Wu (2007). Fire whirls due to surrounding flame sources and the influence of the rotation speed on the flame height. *Journal of Fluid Mechanics* 583, 313–345.